Computers and Electronics in Agriculture 171 (2020) 105234

Contents lists available at ScienceDirect

Computers and Electronics in Agriculture

journal homepage: www.elsevier.com/locate/compag

Comparison of machine learning methods for citrus greening detection on UAV multispectral images

Yubin Lan[a,b], Zixiao Huang[b,c], Xiaoling Deng[a,b,*], Zihao Zhu[b,c], Huasheng Huang[b,c], Zheng Zheng[d], Bizhen Lian[a,b], Guoliang Zeng[a,b], Zejing Tong[b,c]

[a] College of Electronic Engineering, South China Agricultural University, Guangzhou 510642, China
[b] National Center for International Collaboration Research on Precision Agricultural Aviation Pesticide Spraying Technology, Guangdong, China
[c] College of Engineering, South China Agricultural University, Guangzhou 510642, China
[d] College of Agriculture, South China Agricultural University, Guangzhou 510642, China

ARTICLE INFO

Keywords:
Citrus HLB detection
UAV
Multispectral images
Machine learning

ABSTRACT

Citrus Huanglongbing (HLB), also known as citrus greening, is the most destructive disease in the citrus industry. Detecting this disease as early as possible and eradicating the roots of HLB-infected trees can control its spread. Ground diagnosis is time-consuming and laborious. Large area monitoring method of citrus orchard with high accuracy is rare. This study evaluates the feasibility of large area detection of citrus HLB by low altitude remote sensing and commits to improve the accuracy of large-area detection. A commercial multispectral camera (ADC-lite) mounted on DJI M100 UAV(unmanned Aerial Vehicle) was used to collect green, red and near-infrared multispectral image of large area citrus orchard, a linear-stretch was performed to remove noise pixel, vegetation indices (VIs) were calculated followed by correlation analysis and feature compression using PCA (principal components analysis) and AutoEncoder to discover potential features. Several machine learning algorithms, such as support vector machine (SVM), k-nearest neighbour (kNN), logistic regression (LR), naive Bayes and ensemble learning, were compared to model the healthy and HLB-infected samples after parameter optimization. The results showed that the feature of PCA features of VIs combining with original DN (digital numbers) value generally have highest accuracy and agreement in all models, and the ensemble learning and neural network approaches had strong robustness and the best classification results (100% in AdaBoost and 97.28% in neural network) using threshold strategy.

1. Introduction

Citrus huanglongbing (HLB) is the most destructive disease that affects citrus growth because of its harmfulness and rapid spread. Nowadays, the most common detection method of citrus HLB is conducted by naked eyes diagnosis in the field (Wang and Deng, 2008). This method is subjective, time-consuming and laborious. Polymerase chain reaction (PCR) diagnosis is currently the most reliable and objective detection method, however, it is also time-consuming and high-cost as it requires specialised equipment and professional staff. In large-area orchard, it is nearly impossible to manually inspect all citrus tree. Therefore, it is of great significance to develop a timely and effective method to prevent and control the spread of citrus HLB in a large scale so that improve the quality and yield of citrus produce.

Several remote sensing techniques, such as hyperspectral data from airborne (Zhang, 2003; Ye, 2008; Lan,2019) and satellite platforms (Ustin, 2004; Li, 2015) using multispectral (Hunt et al., 2006) and optical imagery (Huang, 2019; Deng, 2016a; Chaoying et al., 2018), were proposed for different agricultural applications. These techniques commonly generate substantial datasets, proper and effective advanced algorithms and high-power computation are necessary to analyse them. Machine learning methods are a powerful tool to address this problem. For example, Weng et al. (2018) successfully utilised a least squares-support vector machine (LS-SVM) classifier to analyse hyperspectral images of healthy, HLB-infected (asymptomatic and symptomatic), and nutrient-deficient leaves. The results achieved 90.2%, 96.0%, and 92.6% classification accuracies during the cool season, hot season, and overall, respectively. Deng (2014) proposed that the HLB recognition accuracy can reach 95–100% within 1s with a Gaussian mixture model-based object and feature extraction method. Deng et al. (2016a, 2016b) also proposed a detection method for citrus HLB based on several colour and texture features extracted from visual imagery and a two-stage back

* Corresponding author at: College of Electronic Engineering, South China Agricultural University, Tianhe District, Guangdong 510642, China.
E-mail address: dengxl@scau.edu.cn (X. Deng).

https://doi.org/10.1016/j.compag.2020.105234
Received 22 July 2019; Received in revised form 12 January 2020; Accepted 17 January 2020
Available online 27 February 2020
0168-1699/ © 2020 Elsevier B.V. All rights reserved.

propagation neural network (BPNN) model, which reached an approximate 92% discrimination accuracy. Mei et al. (2014) presented a partial least square discriminate analysis (PLS-DA) model to handle hyperspectral data after pre-processing using Savitzky-Golay smoothing with first derivative methods and achieved a classification accuracy of more than 96.4%. Lu et al. (2017) utilised three classification discriminant analysis algorithms (fisher discriminant analysis (FDA); stepwise discriminant analysis (SDA); and kNN) to detect anthracnose crown rot in strawberries. They achieved classification accuracies of 71.3%, 70.5% and 73.6% for the SDA, FDA and kNN, respectively.

Compared with satellite and manned aircraft remote sensing, unmanned aerial vehicle (UAV) remote sensing technology has high flexibility as the altitude can be adjusted based on the different spatial and spectral resolution requirements for different tasks. Recently, research around the world regarding crop management based on UAV remote sensing image information and spraying has made great progress (Chaoying et al., 2018; LAN,2019). Swain et al. (2010) proposed that an unmanned helicopter-based, low-altitude remote sensing platform can substitute for satellite-based and costly manned airborne remote sensing methods to estimate yield and biomass. Liu et al. (2018) employed UAV imagery to detected wheat powdery mildew, and a relationship between the image parameter lgR (Red band value logarithmically transformed on the base of 10) and the disease severity was observed by capturing UAV imagery at different altitudes over the wheat fields.

For citrus HLB detection, some non-destructive methods have also been recently proposed based on optical and spectroscopic methods. Qin et al. (2009) proposed that analysing hyperspectral wavelengths between 450 and 930 nm, coupled with spectral information with a divergence-based image classification method, could detect citrus canker with a classification accuracy of 95% under indoor conditions. Kumar et al. (2012) achieved an 80% accuracy in HLB detection using a mixture tuned matched filters on hyperspectral images with an 87% accuracy using spectral angle mapping on multispectral images. Lee et al. (2014) proposed the ESAM method that uses the Savitzky-Golay smoothing filter to remove spectral noise, SVM to build a mask to separate the tree canopy and the background, and vertex component analysis to choose pure endmembers and the red-edge position to filter out most of the false positive detections after a spectral angle mapping (SAM). The method provided the highest detection accuracy of more than 80% in the calibration set and 86.3% in the validation set for hyperspectral imagery, while most of the tree canopies under shadows were misclassified in the multispectral imagery. Sankaran et al. (2011) used a portable spectrometer (visible-near-infrared) to detect HLB disease in citrus trees. The reflectance data were analysed as first and second derivatives, while the overall classification accuracy of the detection system was more than 90%. Similarly, Mishra et al. (2012) utilised visible-near-infrared spectroscopy and three classification methods (kNN, LR, and SVM) to detect HLB in tree canopies with more than 90% accuracy. Sankaran and Ehsani (2013) achieved more than 90% classification accuracy by developing a technique to distinguish healthy citrus leaves from leaves affected with canker and HLB using portable spectroscopy (visible-near-infrared and mid-infrared) and two classifiers (quadratic discriminant analysis and kNN). Abdulridha et al. (2019) developed a hyperspectral (400–1000 nm) imaging system in the laboratory to detect citrus canker in asymptomatic, early, and late stage disease developments on Sugar Belle leaves and immature (green) fruit using the radial basis function (RBF) and kNN. The results indicate that the overall classification accuracy of the RBF was higher than the kNN method for detecting canker in leaves, but detecting canker in fruit was more difficult in the early stages.

The classification results may vary significantly with different feature processes and machine learning algorithms. However, there are few studies on the performance comparison of different feature extraction and learning methods based on the multi-spectral image collected by UAV, and the research on the accuracy improvement of for citrus HLB detection based on UAV remote sensing is also very rare. This study is aimed at investigating feature pre-processing, feature extraction, machine learning models and accuracy improvement on UAV multispectral images so as to explore an effective, non-destructive in-field detection of citrus HLB in a large-area scale. Our code and models are available at: https://github.com/zixiaohuang/Project1_code.

2. Data collection

2.1. Field plot

The experiments were performed from 12.00 a.m. to 3.30 p.m. on 19 December 2017 at a citrus orchard in Huizhou, Guangdong province (N23°49′95.0163″, E114°46′91.0973″). The weather was sunny with no clouds. The field plot was planted with plant spacing of 2.5 m and row spacing of 4 m. There were totally 334 citrus plants, divided into healthy and HLB-infected trees. The degree of HLB infected tress was confirmed in the HLB Research Laboratory of South China Agricultural University by PCR test. Although there were various degrees of HLB, this study categorized them into a single group of HLB infection.

2.2. Data collection

Matrice 100 UAV (produced by China DJI Company) was adopted as the low-altitude remote sensing platform, and a multi-spectral camera (ADC-lite) was mounted on DJI M100 UAV to collect the data of the orchard. The specification of the camera is shown in Table 1.

A whiteboard calibration of the camera was performed. The flight altitude was 60 m, the flight speed was 2–3 m/s and the forward and side laps were both set to 60% during the experiments. The flight routes were generated using the software of the ground station (DJI GS PRO). During data collection, autonomous flight was performed according to the planned route.

2.3. Data pre-processing

The PixelWrench2 software was used to reconstruct the raw images to produce a set of JPG images. The images and GPS position files were imported into the software Agisoft PhotoScan to stitch the images together and build a panorama. The images were cropped after stitching and enhanced in the software ENVI. Similar to the Savitzky-Golay smoothing filter methods from Li et al. (2014), linear stretching was used for preliminary image denoising which removed abnormal DN value that were less than 2% and greater than 98%. The image after pre-processing is shown as Fig. 1 (combinations of the orders of Green, Red and NIR band). The red circles were manually marked and represent the diseased plants, which were pre-marked and confirmed by PCR testing.

Table 1
Specification of the multispectral image acquisition system.

Device	Specification	
Tetracam ADC-lite	Resolution	2048×1536 pixels
	Wavelength range (3 channels)	Green: 520–600 nm Red: 630–690 nm NIR (Near Infrared): 760–900 nm
	Dimension	114 × 77 × 22mm
	Weight	0.2 kg
	Lens size	8 mm/4.5–10 mm
	Field of view	42.5°×32.5°
Calibration whiteboard	Reflectivity	100%
	size	50×50 cm

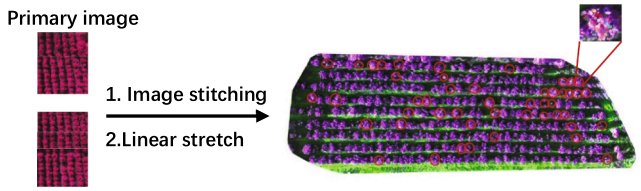

Fig. 1. Multi-spectral image pre-processing and labelling.

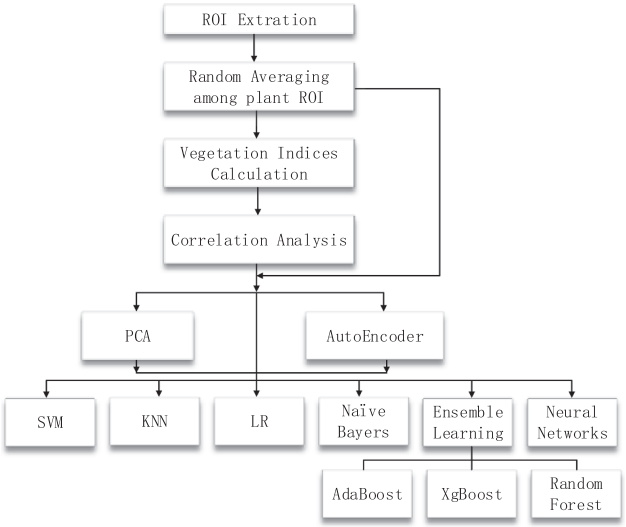

Fig. 2. The framework of the study.

3. Methodology

Fig. 2 shows the framework of this study, the detail of each process is introduced later in this section. Six machine learning algorithms, the SVM (Cortes, 1995), kNN (Fukunaga, 2013), LR (Larose, 2006), naïve Bayes, neural network (Haykin,1994), ensemble learning (Polikar, 2006) including random forest (Breiman, 2001), Adaptive Boosting (Freund et al., 1999) and Xgboost (Chen, 2016) were compared in terms of their feasibility of classification after individually optimising their different parameters. All the algorithms were implemented using Python 3.6.

3.1. ROI extraction and samples production

Using ENVI software, the region of interest was extracted from the center of the canopy of diseased and healthy plants according to an equidistant distribution. 27 diseased trees and 27 healthy ones were selected from Fig. 1, 30 ROIs were manually extracted from each plant. The radius of each ROI was set as 5 pixels (one example of ROI feature extraction is shown in the upper right panel of Fig. 1). The intensity value of the three bands (near-infrared, red and green) were exported from each ROI in the ENVI software. Fig. 3 shows the ROI average intensity comparison between the healthy and HLB-infected group. The red band intensity within the ROI of healthy plants is lower than the one of HLB-infected, while the NIR and green bands have the opposite behaviour.

Due to the uneven distribution of HLB symptom on a plant, the characteristics of different ROIs in the same tree show slight differences. To augment the scale and robustness of the datasets, 5 randomly selected ROIs from 30 ROIs were averaged to product a sample data. Thus, totally 7,695,324 samples including HLB-infected and healthy ones were produced as the datasets in this study.

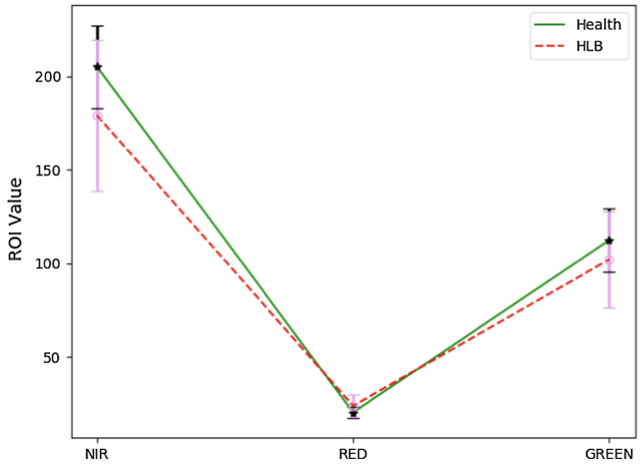

Fig. 3. ROI mean intensity with the standard deviation indicated by the bars.

3.2. Vegetation indices calculation

To enhance the plant characteristic information (Abdulridha, 2019), VIs were adopted to provide additional features in this study. 20 VIs were computed from the DN value of three bands. The definitions of these VIs are shown in Table 2. The NDVI, SIPI, TVI, DVI, RVI, SR, G, MCARI1, MTVI-1, MTVI-2 and RDVI were suggested by some in the HLB field (Mishra et al., 2011, 2009). Other VIs (GDVI, OSAVI, NDGI, IPVI, CVI, GRNDVI, Normal R, Normal NIR and Normal G) were also popularly used in remote sensing.

3.3. Feature extraction

To the best of our knowledge, most studies use all the VIs directly as features. In this study, a correlation analysis and feature compression of the VIs in Table 2 was conducted to remove redundancy and extract lower relevant features. Each sample was composed of multi-dimensional VIs features; therefore, all the samples can be formed as a matrix X. The Pearson product-moment correlation coefficient (shown in Equation 1–4) was adopted to analyse the correlation for different VIs. $\mathbf{X}_i$, $\mathbf{X}_j$ respectively represent VIs feature i and j in the matrix, and the outcome η was ranged between 0 and 1 (Equation (5)). The closer η to 1, the higher linearly correlation of the VIs is, thus one of them should be removed as its high redundancies.

$$\eta = \frac{\mathrm{cov}(\mathbf{X}_i, \mathbf{X}_j)}{\sqrt{\mathrm{var}(\mathbf{X}_i) \bullet var(\mathbf{X}_j)}} \tag{1}$$

$$\mathrm{cov}(\mathbf{X}_i, \mathbf{X}_j) = E[(\mathbf{X}_i - E(\mathbf{X}_i))(\mathbf{X}_j - E(\mathbf{X}_j))] \tag{2}$$

$$\mathrm{var}(\mathbf{X}_i) = E[(\mathbf{X}_i - E(\mathbf{X}_i))^2] \tag{3}$$

$$\mathrm{var}(\mathbf{X}_j) = E[(\mathbf{X}_j - E(\mathbf{X}_j))^2] \tag{4}$$

$$\eta \rightarrow \eta \times 0.5 + 0.5 \tag{5}$$

PCA is mathematically defined as a linear orthogonal transformation that transforms the data into a new coordinate system such that the component with the greatest variance by some projection of the data becomes the first principal component; the second greatest variance is the second principal component and so on (Jolliffe et al, 2011). An AutoEncoder (Liou et al, 2014) consists of two parts: encoder and decoder. The encoder stage ϕ learns to compress input data $\mathbf{x} \in \mathbb{R}^d = \mathbf{X}$ and map it into $\mathbf{h} \in \mathbb{R}^p = \mathbf{F}$ (shown in Eqs. (6) and (7)), and the decoder stage ψ decompresses $\mathbf{h}$ into the reconstruction $\mathbf{x}'$ that closely matches the original data, which is finally trained to minimise the reconstruction errors from "losses" (Eqs. (8) and (9)). The structure of the encoder consists of three sub-modules based on the Conv-BatchNorm-

Table 2
Definition of selected VIs.

Vegetation index equation	References
NormalisedDifferenceVegetationIndex(NDVI) = (NIR − RED)/(*NIR* + *RED*)	Peñuelas et al., 1997
StructureIntensivePigment(SIPI) = (NIR − GREEN)/(NIR + RED)]	Peñuelas *et al.*, 1995
TriangularVegetationIndex(TVI) = 0.5[120(NIR − GREEN) − 200(RED − GREEN)]	Haboudane et al., 2004
DifferenceVegetationIndex(DVI) = NIR − RED	Becker et al., 1988
DifferenceNIR/GreenDifferentVegetationIndex(GDVI) = NIR − GREEN	Tucker et al., 1979
OptimiisedSoil − AdjustedVegetationIndex (OSAVI) = $(NIR - RED) * \frac{1+L}{NIR+RED+L}$; $L = 0.16$	Rondeaux et al., 1996
RatioVegetationIndex(RVI) = NIR/RED	Jordan et al., 1969
SimpleRationIndex(SR) = NIR/GREEN	Daughtry et al., 2000
GreenIndex(G) = GREEN/RED	Clevers *et al.*, 1989
NormalizedDifferenceGreennesIndex(NDGI) = (GREEN − RED)/(GREEN + RED)	Chamadn *et al.*, 1991
InfraredPercentageVegetationIndex(IPVI) = NIR/(NIR + RED)	Crippen et al., 1990
ChlorophyllVegetationIndex(CVI) = $(NIR * RED)/(GREEN)^2$	Vincini et al., 2008
ModifiedChlorophyllAbsorptioninReflectanceIndex(MCARI1) = 1.2 ∗ [2.5 ∗ (NIR − RED) − 1.3 ∗ (NIR − GREEN)]	Daughtry et al., 2000
ModifiedTriangularVegetationIndex − 1(MTVI1) = 1.2 ∗ [1.2 ∗ (NIR − GREEN) − 2.5 ∗ (RED − GREEN)]	Haboudane et al., 2004
ModifiedTriangularVegetationIndex − 2(MTVI2) = $\frac{1.5[1.2(NIR-GREEN)-2.5*(RED-GREEN)]}{\sqrt{(2*NIR+1)^2-(6*NIR-5*\sqrt{RED})-0.5}}$	Smith et al., 2008
RenormalizedDifferenceVegetationIndex(RDVI) = $\frac{(NIR-RED)}{\sqrt{(NIR+RED)}}$	Roujean et al., 1995
GreenRedNormalizedDifferenceVegetationIndex(GRNDVI) = (NIR − RED − GREEN)/(NIR + RED + GREEN)	Wang et al., 2007
NormalizedRedBandIndex(NormR) = RED/(NIR + RED + GREEN)	Original formula
NormalizedNear − InfraredBand(NormNIR) = NIR/(NIR + RED + GREEN)	Original formula
NormalizedGreenBandIndex(NormG) = GREEN/(NIR + RED + GREEN)	Original formula

LeakyRelu. The structure of the decoder consists of the same number of sub-modules based on the DeConv-BatchNorm-Relu. The activation function is ReLU function (Eq. (10)), the loss function is the Mean Squared Error (Eq. (9)) and the Adam algorithm is chosen to optimise the iteration. Dropout is a regularisation technique to reduce overfitting in neural networks (Hinton et al, 2016). However, the loss, in this case, was not improved by using dropout after the input layer or between the input layer and the hidden layers in this study.

$$\phi: \mathbf{X} \rightarrow \mathbf{F}, \mathbf{h} = \sigma(\mathbf{W}\mathbf{x} + \mathbf{b}) \tag{6}$$

$$\psi: \mathbf{F} \rightarrow \chi, \mathbf{x}' = \sigma'(\mathbf{W}'\mathbf{h} + \mathbf{b}') \tag{7}$$

$$\phi, \psi = \underset{\phi,\psi}{\operatorname{argmin}} \|X - (\psi^{\circ}\phi)X\|^2 \tag{8}$$

$$L(\mathbf{x}, \mathbf{x}') = \|\mathbf{x} - \mathbf{x}'\|^2 \tag{9}$$

$$\sigma(x), \sigma'(x) = \max(0, x) \tag{10}$$

where σ, σ' is activation function, $\mathbf{W}, \mathbf{W}'$ is a weight matrix and $\mathbf{b}, \mathbf{b}'$is a bias vector, L is loss function.

Unlike PCA, AutoEncoder was a non-linear compression. For a direct comparison, this study compared PCA with AutoEncoder to extract fewer VI features.

3.4. Learning methods optimization

As the parameters of each machine learner have a great impact on performance, parameters of each leaner need to be determined so that the most accurate and robust classifiers can be obtained. These parameters are summarised in Table 3. GridSearch method in sklearn was used for parameter optimization of the different algorithms based on the experimental results. While some of the algorithms were time-consuming, the study tried to run the jobs in parallel for all CPU kernels to accelerate the calculation speeds.

To SVM, the penalty C and kernel function are needed to be optimized: penalty C was searched for the optimal value from 0.01 to 1000 with 10 steps, and the degree was searched from 1 to 3 in polynomial kernel, and the gamma value was searched from 0 to 1000 with 10 steps in Gaussian kernel. To kNN, the neighbour number was searched in odd value from 3 to 2000, and the leaf size in kd-tree algorithm was searched from 30 to 1000 with 50 steps, the samples weights based on uniform or distance were also compared. To LR, L1 and L2 regularization were compared, and the optimized function was compared among quasi-newton, stochastic average gradient descent and newton with hessian matrix. For the neural network classifier, we searched the classifier with various combination: hidden layer numbers ranging from 2 to 3 and neuron number from 8 to 64. The activation function was searched among sigmoid, tanh, relu; and the optimizer function was searched among gradient decent, quasi-newton, adam algorithm (Kingma and Ba, 2014). The learning rate was set as adaptive mode. To decision tree and ensemble learning, the depth of tree was searched from 2 to 150, and the minimum samples number in each leaf node was searched from 1 to 4, the min samples number to split a new node was searched from 2 to 30, the maximum nodes, maximum samples and features of the nodes all have no limit, and the estimator number was searched from 30 to 500 in ensemble learning. The study uses the CART algorithm, which obtains higher accuracy than the ID3 algorithm in the experiment.

4. Results and discussions

4.1. Comparison of different feature extraction methods

We tried to retain enough features without redundancy, thus, only when the correlation result between two VIs is near to 1.0 (highly linear correlation), one of these two VIs will be removed. The results of the correlation analysis for various VIs are shown in Fig. 4. For example, OSAVI and IPVI were highly linear correlated with NDVI, we removed OSAVI and IPVI and reserve NDVI. Similarly, TVI and SIPI, MCARI1 and MTVI1, DVI and MTVI1, GRNDVI and Norm NIR also have highly linear correlation with each other, we removed TVI, MCARI1, DVI and GRNDVI.

Table 3
Algorithm parameters.

Algorithm		Hyper-parameter tuning					
SVM		Penalty C	Kernel function (linear/polynomial/gaussian)				
kNN		K Neighbors	Weights(uniform/distance)		Leaf size		
LR		L1/l2 Regularization		Optimize function			
Naïve Bayer		Bernoulli/Gaussian/Polynomial					
Neural Network		Hidden layer	Neuros numbers	Activation function	Learning rate	Optimize function	
Decision Tree		ID3/C4.5/CART	Max depth	Min leaf node samples	Min split samples	Max leaf nodes	
Ensemble Learning	Random Forest	ID3/C4.5/CART	Max depth	Min leaf node samples	Min split samples	Max leaf nodes	Estimator numbers
	Adaptive Boosting	Base Estimator	Estimator numbers	Learning rate			
	Xgboost	Linear/tree booster	Estimator numbers	Max depth	Learning rate	Min child leaf weight	gamma
		Max leaf nodes	subsamples				

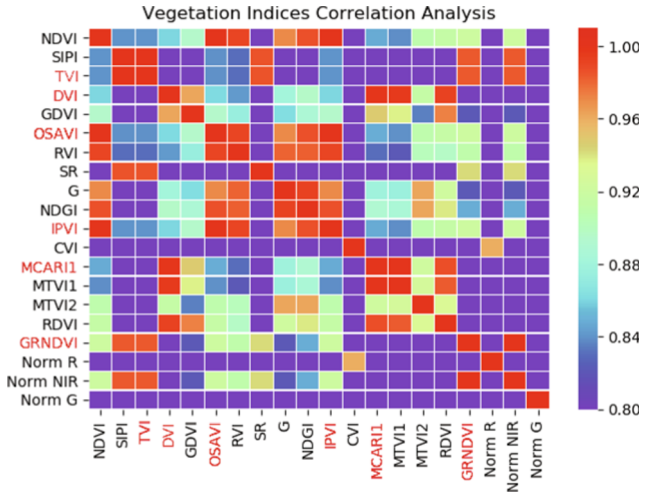

Fig. 4. Correlation analysis heat map.

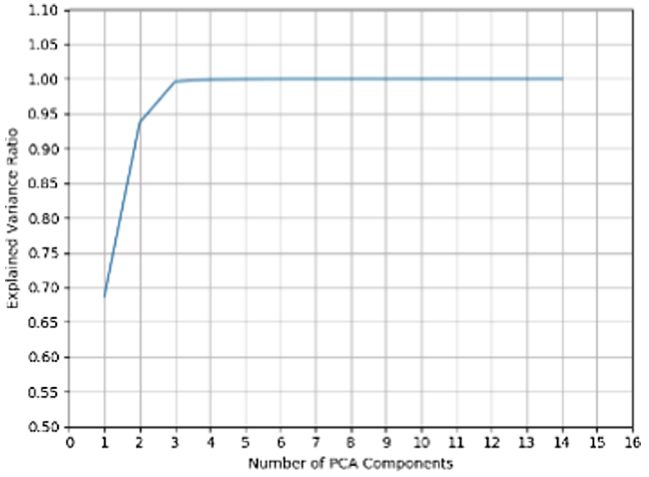

Fig. 5. Explained variance ratio for PCA.

The result of PCA linear compression with different number components are shown in Fig. 5, it is shown that the data after dimension reduction can retain more than 99.9% of the variance information when the original data are compressed into three or more features by PCA. Therefore, 3 components were chosen in the PCA scheme of feature extraction in this study.

For a direct comparison with the PCA, AutoEncoder was also used to compress the original data into 3 dimensions. The comparison between AutoEncoder and PCA is shown in Fig. 6. The green dots represent the healthy samples distribution while the red triangles are the HLB-infected samples. From Fig. 6, the two groups can be separated by naked eyes although there are some outliers which might be affected by environment or the uneven appearance of the leaves.

4.2. Comparison of different machine learning methods

4.2.1. Classification assessment

The classification assessment measures (Eqs. (11)–(15)), including accuracy, recall, precision, specificity and F1-score, are calculated from the Table 4 confusion matrices (Kenney and Keeping, 1957; Sankaran et al., 2013). The precision and specificity represent the classification accuracies of the healthy and HLB samples, respectively, and the accuracy represents the percentage of correctly classified healthy and HLB samples. The F1-score is a combination of the recall and the precision. A higher F1-score indicates a more robust classification model.

$$\text{Accuracy}(\%) = \frac{TN + TP}{TN + TP + FN + FP} \times 100 \tag{11}$$

$$\textit{Specificity}(\%) = \frac{TN}{TN + \text{FP}} \times 100 \tag{12}$$

$$\text{Recall}(\%) = \frac{TP}{TP + FN} \times 100 \tag{13}$$

$$\text{Precision}(\backslash\% \ ) = \frac{\text{TP}}{\text{TP} + \text{FP}} \times 100 \tag{14}$$

$$\text{F1}(\%) = \frac{2 \times \text{Precision} \times \text{Recall}}{\text{Precision} + \text{Recall}} \times 100 \tag{15}$$

Cohen Kappa (Cohen, 1969) was also introduced to assess the agreement in different algorithm of categorical assessment (Equation 16–18).

$$p_0 = \frac{TN + TP}{TN + TP + FN + FP} \tag{16}$$

$$p_e = \frac{(TP + FP) * (TP + FN) + (FN + TN) * (FP + TN)}{(TP + FP + FN + TN)^2} \tag{17}$$

$$\kappa = \frac{p_0 - p_e}{1 - p_e} \tag{18}$$

where p_0 (Eq. (16)) represents the observed proportional agreement and p_e(Eq. (17)) represents the expected agreement by chance. The value of κ(Eq. (18)) is closer to 1, the better consistency of the model is obtained. When the value is greater than 0.75, the consistency is satisfied, whereas when the value is close to negative 1, the opposite is true. Integrating dimension-reduced datasets with Original reflectance datasets can achieve a better classification result and a faster convergence rate (Deng et al., 2019). Therefore, five sets of the data were chosen and compared: the original reflectance datasets, the datasets by PCA, the datasets by AutoEncoder, the datasets combining original reflectance data and PCA components, and the datasets combining

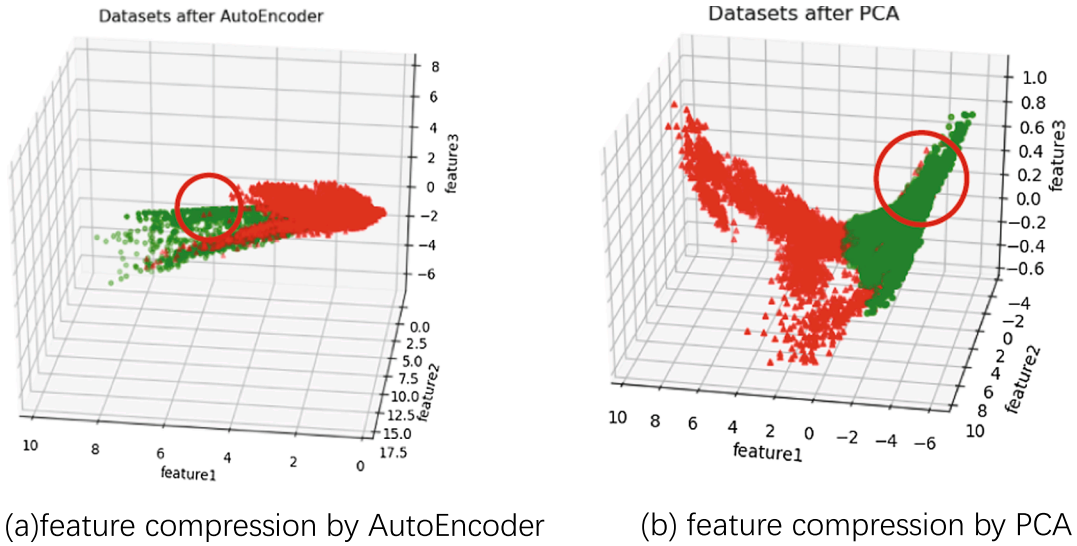

Fig. 6. Comparison of AutoEncoder and PCA for feature compression.

Table 4
Confusion matrix and associated classification measures.

Actual	Predicted	
	Healthy	HLB
Healthy	True Positive (TP)	False Positive (FP)
HLB	False Negative (FN)	True Negative (TN)

original reflectance data and AutoEncoder data. The dimensions of the above datasets are shown in Table 5. The datasets partition ratio for training, validation and testing is shown in Fig. 7. Among the dataset produced by the sample production method in section 3.1, 60% was used for training, 20% was used for parameter validation to optimize the trained model and 20% for testing. There was no intersection among these partitions. The time module of python was used (the temporal resolution was limited to a microsecond) and the mean times for the different algorithms to process the different datasets were recorded for comparison.

4.2.2. Algorithm parameter optimisation

For SVM classifiers, we found that larger degrees in polynomial kernel required much more time with approximately the same accuracy. Therefore, the degree was set to 3 for a comparison with the other kernel functions. The penalty factor C and gamma value of the Gaussian kernel function, both set as 100, could achieve a better score.

The classification results of the SVM approach are shown in Fig. 8. The horizontal axis represents different datasets while the vertical axis represents the classification accuracy results. From Fig. 8(a)–(e), the classification accuracy varies with different datasets and different kernel functions. Generally, feature extraction (PCA, AutoEncoder) slightly improved the classification results, especially with the polynomial kernel and Gaussian kernel. Inserting the original reflectance data into the datasets after feature extraction further improved the classification results. The graph in Fig. 8(d) reflects that the polynomial kernel averagely cost much more time than the others, and adding the original reflection data can accelerate the convergence time. Fig. 8(e) reveals that PCA combine original reflection datasets have highest agreement in different models. Overall, the Gaussian kernel got the best classification accuracy and agreement among the three SVM kernels.

For kNN classifiers, the leaf size of KD-tree was selected as 30. The optimal number of neighbouring points set about 7 generated the best classification accuracy. The Euclidean distance obtained a better accuracy in the case of uniform weights, whereas the distance weight performed better for the Manhattan distance. The analysis results for the different datasets are shown in Fig. 9(a). It can be seen from the figure that the classifiers have similar accuracy between uniform and distance weight, and PCA features with original reflectance data also performed better than the others.

For LR classifiers, the L2 regularisation had a higher score than the L1 regularisation. The stochastic average gradient solver was selected to optimise the loss function as this algorithm can attain better results for large datasets. The classification results are shown in Fig. 10(a), the ability of LR models to distinguish HLB-samples seem worse than health one (The specificity score is much lower than the others).

For the naïve Bayes classifier, it is apparent from Fig. 11(a) that the AutoEncoder feature had a substantial drop in the classification accuracy results compared with other datasets. It is also seen from the graph in Fig. 11(b) that the Bernoulli naïve Bayes had even worse results when detecting HLB-infected samples after feature extraction. Overall, the naïve Bayes classifier have a poor classification result in this study and the Gaussian naïve Bayes generally had better classification accuracy while the nonlinear features had worst results.

For the decision tree classifier, the CART algorithm with the Gini impurity obtained a better score than the ID3 algorithm based on the information gain. And the depth of the tree is selected as 8. The classification results for the decision tree algorithm are shown in Fig. 12. The graph in Fig. 12(a) illustrates an obvious improvement of classification results after adding the original reflectance data to compressed features. Fig. 12(b) indicates that the time dramatically increased for

Table 5
The dimensions and numbers of various datasets.

	Original reflectance Datasets	Datasets after PCA	Datasets after AutoEncoder	Original reflectance + PCA datasets	Original reflectance + AutoEncoder datasets
Dimensions	3	3	3	6	6

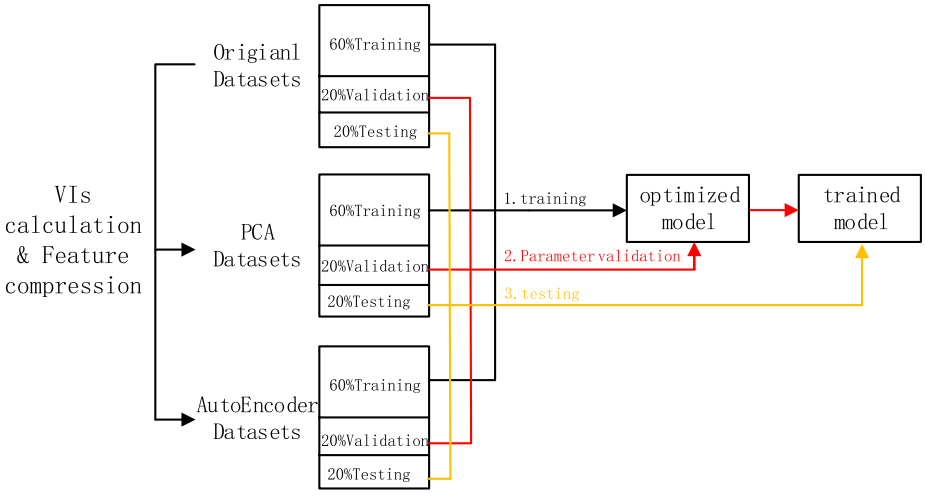

Fig. 7. Feature extraction and data partitioning.

the larger datasets and Fig. 12(c) indicates that the PCA combined with original reflection datasets got the best agreement in different models.

For the ensemble learning classifier, the AdaBoost and the random forest are based on the optimised decision tree algorithm above, the XgBoost is based on the gbtree. As the AdaBoost cannot run in parallel using sklearn, it needs much more time than other algorithms (Fig. 13(d)). The XgBoost pre-orders and stores the data and exploits the sparsity of features to split the node; thus, it is more efficient although it is also unstable (Fig. 13(d)). Overall, these three ensemble learning classifiers got the similar performance, while the AdaBoost using PCA data combing original reflection datasets had a slightly better result.

For the neural network classifier, a better result was achieved with 3 hidden layers and 64,64,8 neuron numbers in layers in sequence among the combination of hidden layer numbers ranging from 2 to 3 and different neuron numbers ranging from 8 to 64. The accuracy achieved to 99.6% with the datasets combining the original data with the PCA data, as shown in Fig. 14(a). A deeper network may achieve better results, but with a cost of a considerable increase in the training time. What's more, the linear feature cost fewer time and higher agreement than non-linear features in neural network classifier.

Overall, the classification result for healthy group was better than the one for the HLB-infected. Both PCA and AutoEncoder features, extracted from original reflectance data, obtained an obviously improvement than primary data, which shows that feature extraction from VIs is beneficial for classification. Also, the linear PCA features have apparent better results than non-linear AutoEncoder feature in each classifier consistently. Therefore, PCA feature extraction was adopted in the later multispectral image analysis process. Compressed features for VIs combining with original reflectance data got the best performance, including the accuracy and agreement. Among the classifiers, neural network and AdaBoost classifiers had considerably better classification accuracies but with much more calculation times.

4.3. Multispectral image analysis

In section 4.2.2, different parameters for the various traditional machining learning algorithms were compared and optimized in ROI level, however, in the practical application, the whole plant is the object of diagnosis and prediction. Thus, in this section, six trained models (SVM with a Gaussian kernel, kNN with a distance weight, LR with an L2 penalty, Gaussian naïve Bayes, AdaBoost with an optimised decision tree and the neural network classifier) were applied to classify each plant in the orthophoto and generate a disease distribution map.

The original reflection datasets were extracted again but in plant level, and the datasets were pre-processed as previously described in Section 2.3. In each plant, totally 30 ROIs were extracted, 5 among these 30 ROIs were randomly averaged so that a total of 142,506 samples for each plant were produced.

A threshold strategy was adopted to determine whether a tree is infected by HLB based on the classification result of all ROIs of it. As the results showed that different models had their own "classification preference." The SVM and LR tended to predict the ROI samples as healthy; the AdaBoost and neural network tended to predict as HLB-infected; while the kNN and Gaussian naïve Bayes were relatively fair. Therefore, different thresholds were set for the models to obtain better classification results for each plant. One example of the classification distribution results based different thresholds with the AdaBoost model is shown in Fig. 15. We clearly see that the classification accuracy steadily increased before reaching a peak and then before declined sharply. As a result, the peak was set as the threshold to determine whether the tree was infected by HLB.

Using the above method, the thresholds for SVM, kNN, LR, Gaussian naïve Bayes, neural network and AdaBoost were set to 65%, 55%, 68%, 58%, 80% and 90% respectively. If the number of ROIs predicted as HLB exceeded the threshold, this plant was considered as infected by HLB. The best classification results of six learners are shown in Fig. 16. The yellow circle indicates false negative, that is, the predicted result

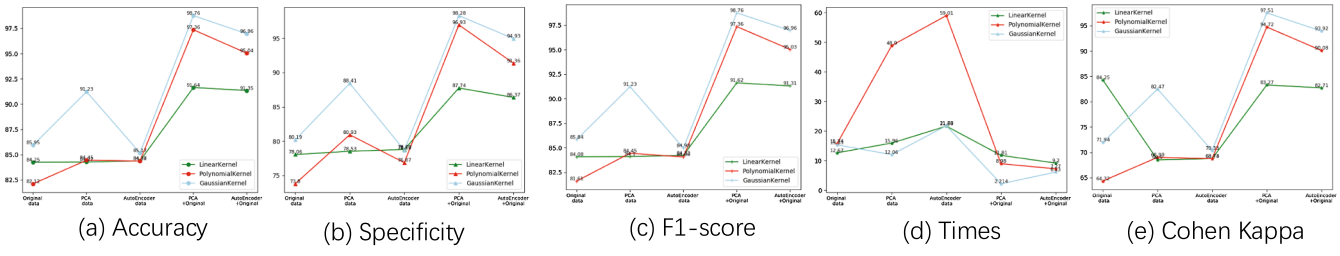

Fig. 8. Classification result for ROIs by SVM with different kernels.

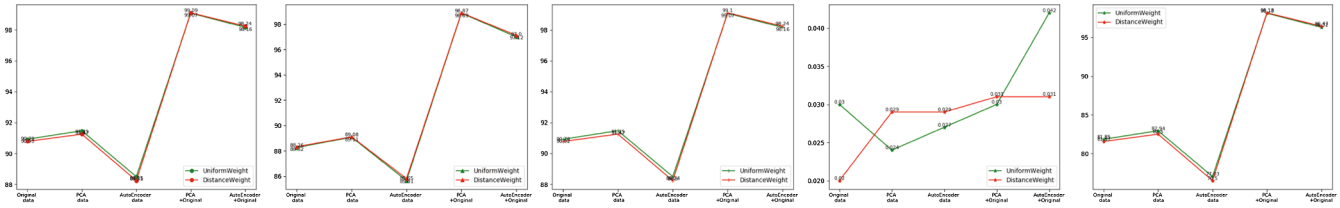

Fig. 9. Classification result for ROIs by kNN with different weights and datasets.

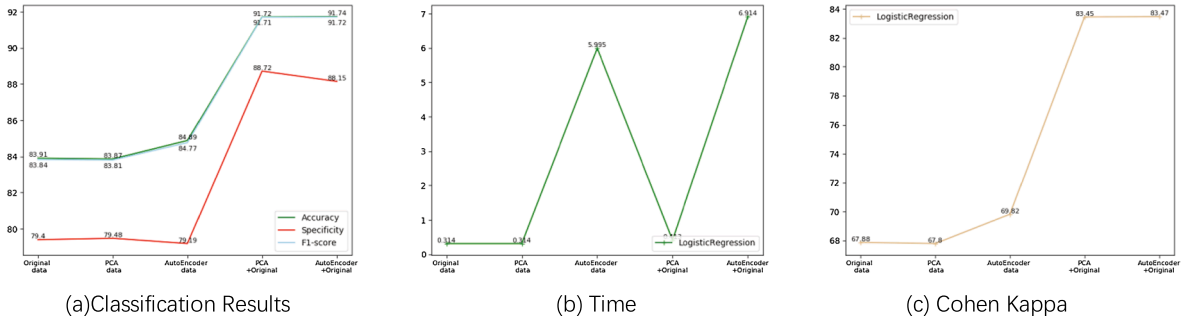

Fig. 10. Classification results for ROIs by LR model with different datasets.

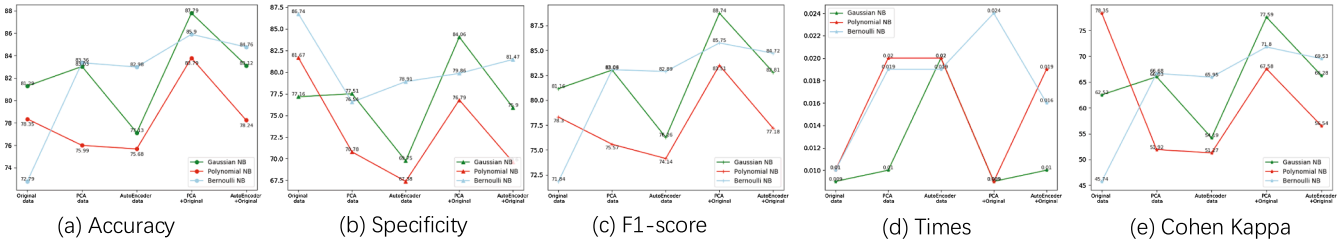

Fig. 11. Classification result for ROIs by naïve Bayes classifiers with different datasets.

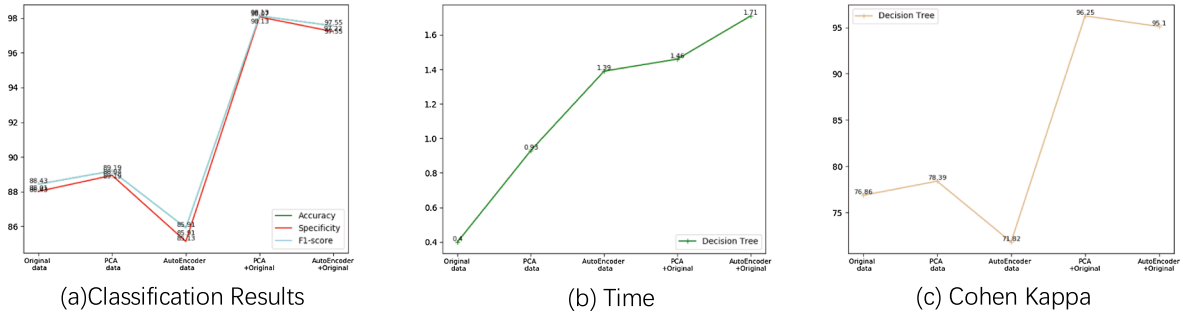

Fig. 12. Classification result for ROIs by decision tree algorithm with different datasets.

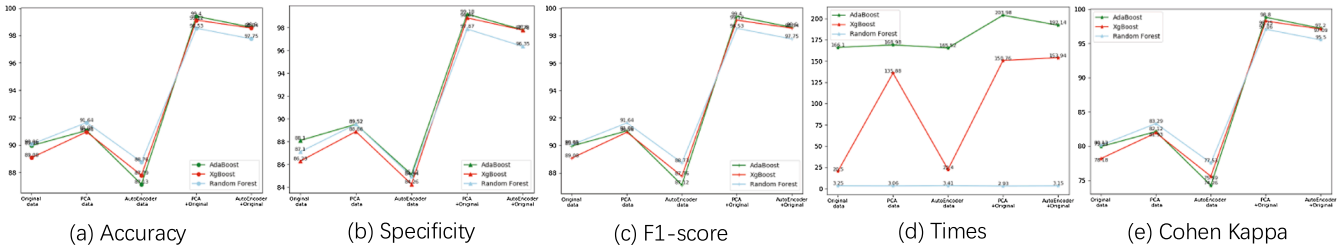

Fig. 13. Classification result for ROIs by ensemble learning with different datasets.

was HLB-infected while the ground truth was healthy, and the red circle indicates false positive, that is, the classifier did not properly predict the HLB plants. Among these classifiers, AdaBoost got an exactly right prediction result in our study, no matter health plants or HLB-infected ones.

More detailed classification information is shown in Table 6. The

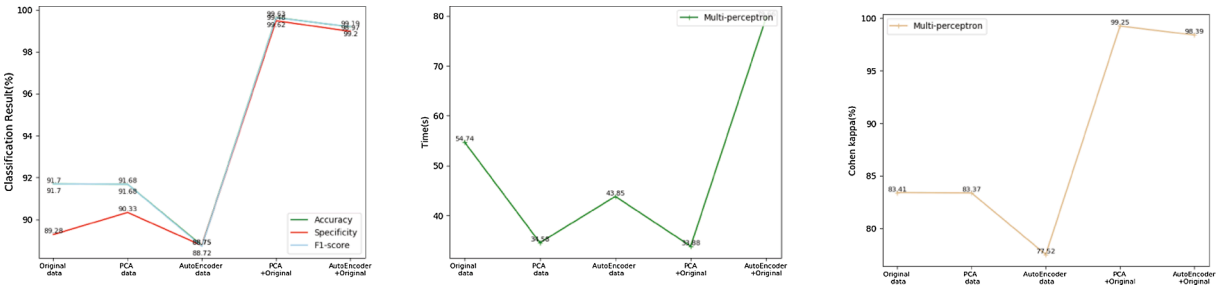

(a)Classification Results (b) Time (c) Cohen Kappa

Fig. 14. Classification result for ROIs by neural network classifier with different datasets.

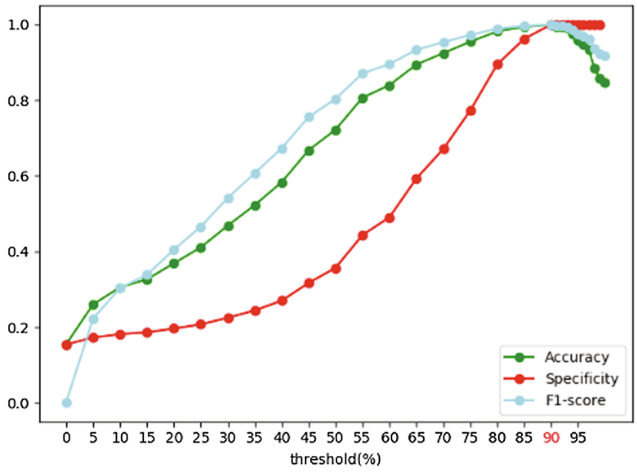

Fig. 15. AdaBoost classification distribution results for different thresholds.

performance of SVM, kNN, LR and naïve Bayes algorithms for detecting HLB plants sharply declined as the predicted samples increased. What's more, it's surprising shown that the Cohen Kappa value in these four models is lower than 75% while AdaBoost and neural network remain high. It means that SVM, kNN, LR and naïve Bayes in our study are easier effected by the samples changing than AdaBoost and neural network. The neural network method remained constant and the AdaBoost maintained the best classification result. Therefore, it is strongly considered that the ensemble learning (AdaBoost) and neural network had good robustness, regardless of the number of samples.

Table 6
Optimised algorithm classification results based on plant.

Algorithm (threshold)	SVM (65%)	kNN (55%)	LR (68%)	Naïve Bayes (58%)	AdaBoost (90%)	Neural network (80%)
Accuracy	79.76	81.27	72.20	80.06	100	97.28
Specificity	33.33	42.47	27.96	34.69	100	88.89
Precision	88.57	85.0	76.07	88.57	100	97.86
Recall	87.63	92.24	89.49	87.94	100	98.91
F1-score	88.10	88.48	82.24	88.26	100	98.38
Cohen Kappa	34.86	50.09	27.12	33.28	100	92.20

5. Discussion and conclusion

5.1. Discussion

To the best of our knowledge, most existing studies used VIs directly to monitor the crop, however, there are a great deal of redundancy particularly when two VIs are highly correlated. In this study, the redundant features were removed by analysing their correlations and the feature dimensions were reduced by linear and nonlinear compression. The result shows that the combination of VIs features compressed and original DN value performed better than the one using DN value individually.

Most existing studies (Lee, 2014; Qin, 2011) showed that multispectral images had rather poorer classification results than

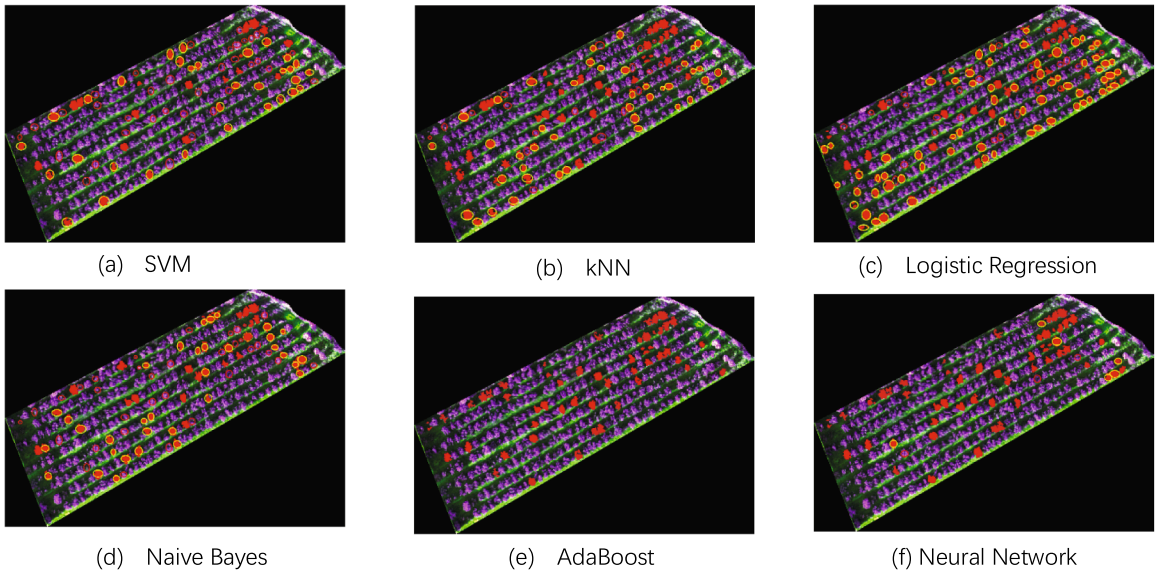

(a) SVM (b) kNN (c) Logistic Regression

(d) Naive Bayes (e) AdaBoost (f) Neural Network

Fig. 16. Classification results in plant level with different algorithms.

hyperspectral images for limited band information available in multispectral images. Therefore, most studies commonly use more suitable hyperspectral images based on band selection to detect citrus HLB. The method proposed in this study proved that multispectral images with NIR, red and green bands can effectively detect HLB under proper feature extraction and classification models. After parameter optimizing and threshold setting, AdaBoost and neural network can accurately classify HLB-infected and health one while the others (SVM, kNN, LR and naïve Bayes) perform worse as the number of predicted samples increasing, and the Cohen Kappa values also reveal that the AdaBoost and neural network had a strongly robustness while SVM, kNN, LR and naïve Bayes were unstable in our study.

This study also explored a strategy to enhance the scale of the datasets by randomly selecting and averaging ROIs intensities, and effectively enriched the information of the original dataset. Nonlinear features performed worse than PCA linear features, no matter in accuracy or time. PCA components datasets combining with original DN value have the highest agreement according to Cohen Kappa. Through tracking the training time, it was proven that the original DN value datasets can effectively accelerate the convergence in some models (SVM, naïve Bayes and neural network).

Although almost perfect classification results were obtained by Adaboost and neural network using PCA features of VIs and original DN value, there are limitations in this study. Firstly, the application scenarios are restricted, as the growth of fruit trees is dynamic, the image data captured in different growing periods represents different features, leading to the performance of the models varies dynamically. It is hard to construct a model to fit every growing period of the citrus. Secondly. The method poses requirements for equipment. There are not standards of band's requirement and whiteboard calibration for multispectral cameras, different multispectral cameras have different band widths, leading the DN value from different equipment also various slightly. For practical application, deeply investigation on regularization and standardization of data should be continued.

5.2. Conclusions

This study explored the potential of UAV multispectral remote sensing method to detect citrus HLB in a large-area scale. Various feature extraction methods were compared using different machine learning algorithms based on multispectral imagery captured by ADC-Lite. The following conclusions can be summarised:

(1) A randomly selected averaging strategy over ROIs can augment the data scale and increase the robustness. A threshold strategy to determine whether plants are infected by HLB based on classification results of ROIs improved the accuracy of plant classification.
(2) Combining the original DN value and the PCA components of VIs features improved the accuracy and accelerated convergence speed of most algorithms.
(3) Linear feature compression performed better than nonlinear compression on representing the feature of citrus HLB.
(4) The ensemble learning and neural network models demonstrate their promising application through better classification results and stronger robustness.

CRediT authorship contribution statement

Yubin Lan: Conceptualization, Methodology, Investigation, Funding acquisition, Project administration, Resources, Writing - original draft. **Zixiao Huang:** Software, Validation, Formal analysis, Visualization, Writing - original draft. **Xiaoling Deng:** Project administration, Supervision, Resources, Methodology, Validation, Formal analysis, Visualization, Writing - original draft. **Zihao Zhu:** Data curation, Writing - review & editing. **Huasheng Huang:** Data curation, Writing - review & editing. **Zheng Zheng:** Resources, Data curation, Validation, Writing - review & editing. **Bizhen Lian:** Data curation, Writing - review & editing. **Guoliang Zeng:** Data curation, Writing - review & editing. **Zejing Tong:** Data curation, Writing - review & editing.

Declaration of Competing Interest

The authors declare that they have no known competing financial interests or personal relationships that could have appeared to influence the work reported in this paper.

Acknowledgements

The research work was supported by the National Natural Science Foundation of China (Grant No. 61675003), the Key-Area Research and Development Program of Guangdong Province (Grant No. 2019B020214003), the Educational Commission of Guangdong Province of China for Platform Construction (Grant No. 2015KGJHZ007) and the Science and Technology Program of Guangzhou, China (Grant No. 201605030013, 201707010346), University Student Innovation Cultivation Program of Guangdong, China (Grant No. pdjh2019b0079), the Leading Talents of Guangdong Province Program (Grant No. 2016LJ06G689) and Science and Technology Planning Project of Guangdong Province (Grant No. 2017B010117010).

References

Fleiss, J.L., Cohen, J., Everitt, B.S., 1969. Large sample standard errors of kappa and weighted kappa. Psychol. Bull. 72 (5), 323.
Wang, Aimin, Deng, Xiaoling, et al., 2008. Research Progress in diagnostic techniques of Citrus Huanglongbing. Guangdong Agric. Sci. 6, 101–103 (in Chinese).
Huang, H., Deng, J., Lan, Y., Yang, A., Zhang, L., Wen, S., Deng, Y., 2019. Detection of Helminthosporium Leaf Blotch Disease Based on UAV Imagery. Appl. Sci. 9 (3), 558.
Ustin, S.L., Roberts, D.A., Gamon, J.A., Asner, G.P., Green, R.O., 2004. Using imaging spectroscopy to study ecosystem processes and properties. Bioscience 54 (6), 523–534.
Hunt, E., Walthall, C., Daughtry, C., Cavigelli, M., Fujikawa, S., Yoel, D. & Tranchitella, M. (2006, March). High-resolution multispectral digital photography using unmanned airborne vehicles. In Biennial Workshop on Aerial Photography, Videography, and High Resolution Digital Imagery for Resource Assessment Proceedings.
Zhang, M., Qin, Z., Liu, X., Ustin, S.L., 2003. Detection of stress in tomatoes induced by late blight disease in California, USA, using hyperspectral remote sensing. Int. J. Appl. Earth Obs. Geoinf. 4 (4), 295–310.
Ye, X., Sakai, K., Sasao, A., Asada, S.I., 2008. Potential of airborne hyperspectral imagery to estimate fruit yield in citrus. Chemometr. Intell. Lab. Syst. 90 (2), 132–144.
Li, X., Lee, W.S., Li, M., Ehsani, R., Mishra, A.R., Yang, C., Mangan, R.L., 2015. Feasibility study on huanglongbing (citrus greening) detection based on WorldView-2 satellite imagery. Biosyst. Eng. 132, 28–38.
Kumar, A., Lee, W.S., Ehsani, R.J., Albrigo, L.G., Yang, C., Mangan, R.L., 2012. Citrus greening disease detection using aerial hyperspectral and multispectral imaging techniques. J. Appl. Remote Sens. 6 (1), 063542.
Liu, W., Cao, X., Fan, J., Wang, Z., Yan, Z., Luo, Y., Zhou, Y., 2018. Detecting wheat powdery mildew and predicting grain yield using unmanned aerial photography. Plant Dis. 102 (10), 1981–1988.
Qin, J., Burks, T.F., Ritenour, M.A., Bonn, W.G., 2009. Detection of citrus canker using hyperspectral reflectance imaging with spectral information divergence. J. Food Eng. 93 (2), 183–191.
Li, H., Lee, W.S., Wang, K., Ehsani, R., Yang, C., 2014. 'Extended spectral angle mapping (ESAM)'for citrus greening disease detection using airborne hyperspectral imaging. Precis. Agric. 15 (2), 162–183.
Weng, H., Lv, J., Cen, H., He, M., Zeng, Y., Hua, S., He, Y., 2018. Hyperspectral reflectance imaging combined with carbohydrate metabolism analysis for diagnosis of citrus Huanglongbing in different seasons and cultivars. Sens. Actuators, B 275, 50–60.
Lu, J., Ehsani, R., Shi, Y., Abdulridha, J., de Castro, A.I., Xu, Y., 2017. Field detection of anthracnose crown rot in strawberry using spectroscopy technology. Comput. Electron. Agricul. 135, 289–299.
Sankaran, S., Mishra, A., Maja, J.M., Ehsani, R., 2011. Visible-near infrared spectroscopy for detection of Huanglongbing in citrus orchards. Comput. Electron. Agric. 77 (2), 127–134.
Mishra, A.R., Karimi, D., Ehsani, R., Lee, W.S., 2012. Identification of citrus greening (HLB) using a VIS-NIR spectroscopy technique. Trans. ASABE 55 (2), 711–720.
Abdulridha, J., Batuman, O., Ampatzidis, Y., 2019. UAV-based remote sensing technique to detect citrus canker disease utilizing hyperspectral imaging and machine learning. Remote Sens. 11 (11), 1373.

Chaoying, T.A.N.G., Xianghui, W. E. I., Biao, W. A. N. G., & PRASAD, S. (2018). A Cross-Border Detection Algorithm for Agricultural Spraying UAV.
Swain, K.C., Thomson, S.J., Jayasuriya, H.P., 2010. Adoption of an unmanned helicopter for low-altitude remote sensing to estimate yield and total biomass of a rice crop. Trans. ASABE 53 (1), 21–27.
Yubin Lan, Zihao Zhu, X Deng et al. (2019). Monitoring and Classification of Citrus Huanglongbing Plants Based on UAV Hyperspectral Remote Sensing. Transactions of the Chinese Society of Agricultural Engineering, 35(3):92-100(In Chinese).
Deng, X., Lan, Y., Xing, X., Mei, H., Liu, J., Hong, T., 2016. Detection of citrus huanglongbing based on image feature extraction and two-stage BPNN modeling. Int. J. Agric. Biol. Eng. 9 (6), 20–26.
Deng, X.L., Li, Z., Hong, T.S., 2014. Citrus disease recognition based on weighted scalable vocabulary tree. Precis. Agric. 15 (3), 321–330.
Deng, X., Huang, Zixiao, Zheng, Zheng, Lan, Yubin, Dai, Fen, 2019. Field detection and classification of citrus Huanglongbing based on hyperspectral reflectance. Comput. Electron. Agric. 167, 105006. https://doi.org/10.1016/j.compag.2019.105006.
Deng, X., Lan, Y., Hong, T., Chen, J., 2016. Citrus greening detection using visible spectrum imaging and C-SVC. Comput. Electron. Agric. 130, 177–183.
Mei, H., Deng, X., Hong, T., Luo, X., 2014. Early detection and grading of citrushuanglongbing using hyperspectral imaging technique. Trans. Chin. Soc. Agricul. Eng. 30 (9), 140–147.
Peñuelas, J., Isla, R., Filella, I., Araus, J.L., 1997. Visible and near-infrared reflectance assessment of salinity effects on barley. Crop Sci. 37 (1), 198–202.
Jordan, C.F., 1969. Derivation of leaf-area index from quality of light on the forest floor. Ecology 50 (4), 663–666.
Rondeaux, G., Steven, M., Baret, F., 1996. Optimization of soil-adjusted vegetation indices. Remote Sens. Environ. 55 (2), 95–107.
Becker, F., Choudhury, B.J., 1988. Relative sensitivity of normalized difference vegetation index (NDVI) and microwave polarization difference index (MPDI) for vegetation and desertification monitoring. Remote Sens. Environ. 24 (2), 297–311.
Crippen, R.E., 1990. Calculating the vegetation index faster. Remote Sens. Environ. 34 (1), 71–73.
Vincini, M., Frazzi, E., D'Alessio, P., 2008. A broad-band leaf chlorophyll vegetation index at the canopy scale. Precis. Agric. 9 (5), 303–319.
Wang, F.M., Huang, J.F., Tang, Y.L., Wang, X.Z., 2007. New vegetation index and its application in estimating leaf area index of rice. Rice Sci. 14 (3), 195–203.
Haboudane, D., Miller, J.R., Pattey, E., Zarco-Tejada, P.J., Strachan, I.B., 2004. Hyperspectral vegetation indices and novel algorithms for predicting green LAI of crop canopies: Modeling and validation in the context of precision agriculture. Remote Sens. Environ. 90 (3), 337–352.
Tucker, C.J., Elgin Jr, J.H., McMurtrey Iii, J.E., Fan, C.J., 1979. Monitoring corn and soybean crop development with hand-held radiometer spectral data. Remote Sens. Environ. 8 (3), 237–248.
Daughtry, C.S.T., Walthall, C.L., Kim, M.S., De Colstoun, E.B., McMurtrey Iii, J.E., 2000. Estimating corn leaf chlorophyll concentration from leaf and canopy reflectance. Remote Sens. Environ. 74 (2), 229–239.
Smith, A.M., Bourgeois, G., Teillet, P.M., Freemantle, J., Nadeau, C., 2008. A comparison of NDVI and MTVI2 for estimating LAI using CHRIS imagery: a case study in wheat. Canadian J. Remote Sens. 34 (6), 539–548.
Roujean, J.L., Breon, F.M., 1995. Estimating PAR absorbed by vegetation from bidirectional reflectance measurements. Remote Sens. Environ. 51 (3), 375–384.
Mishra, A. R., Ehsani, R. E. Z. A., Karimi, D., & Albrigo, L. G. (2009). Potential applications of multiband spectroscopy and hyperspectral imaging for detecting HLB infected orange trees. In Proceedings of the Florida State Horticultural Society (Vol. 122, pp. 147-151).
Mishra, A., Karimi, D., Ehsani, R., Albrigo, L.G., 2011. Evaluation of an active optical sensor for detection of Huanglongbing (HLB) disease. Biosyst. Eng. 110 (3), 302–309.
Kenney, J.F., Keeping, E.S., 1957. Mathematics of statistics. van Nostrand.
Jolliffe, I., 2011. Principal component analysis. Springer, Berlin Heidelberg, pp. 1094–1096.
Liou, C.Y., Cheng, W.C., Liou, J.W., Liou, D.R., 2014. Autoencoder for words. Neurocomputing 139, 84–96.
Fukunaga, K., 2013. Introduction to statistical pattern recognition. Elsevier.
Larose, D.T., Larose, D.T., 2006. Data mining methods and models. Wiley-Interscience, Hoboken (NJ).
Cortes, C., Vapnik, V., 1995. Support-vector networks. Machine Learn. 20 (3), 273–297.
Polikar, R., 2006. Ensemble based systems in decision making. IEEE Circuits Syst. Mag. 6 (3), 21–45.
Freund, Y., Schapire, R., Abe, N., 1999. A short introduction to boosting. J.-Japanese Soc. Artific. Intell. 14 (771–780), 1612.
Breiman, L., 2001. Random forests. Machine Learn. 45 (1), 5–32.
Chen, T., & Guestrin, C. (2016, August). Xgboost: A scalable tree boosting system. In Proceedings of the 22nd acm sigkdd international conference on knowledge discovery and data mining (pp. 785-794). ACM.
Hinton, G. E., Krizhevsky, A., Sutskever, I., & Srivastva, N. (2016). U.S. Patent No. 9,406, 017. Washington, DC: U.S. Patent and Trademark Office.
Haykin, S., 1994. Neural networks: a comprehensive foundation. Prentice Hall PTR.
Sankaran, S., Maja, J., Buchanon, S., Ehsani, R., 2013. Huanglongbing (citrus greening) detection using visible, near infrared and thermal imaging techniques. Sensors 13 (2), 2117–2130.
Qin, J., Burks, T.F., Zhao, X., Niphadkar, N., Ritenour, M.A., 2011. Multispectral detection of citrus canker using hyperspectral band selection. Trans. ASABE 54 (6), 2331–2341.
Kingma, D.P., Ba, J., 2014. Adam: A method for stochastic optimization. *arXiv preprint arXiv:1412.6980*.